TOPOLOGICAL DERIVATIVES APPLIED TO FLUID FLOW CHANNEL DESIGN OPTIMIZATION PROBLEMS

L. F. N. SÁ, R. C. R. AMIGO, A. A. NOVOTNY AND E. C. N. SILVA

Abstract. Topology optimization methods application for viscous flow problems is currently an active area of research. A general approach to deal with shape and topology optimization design is based on the topological derivative. This relatively new concept represents the first term of the asymptotic expansion of a given shape functional with respect to the small parameter which measures the size of singular domain perturbations, such as holes and inclusions. In previous topological derivative-based formulations for viscous fluid flow problems, the topology is obtained by nucleating and removing holes in the fluid domain which creates numerical difficulties to deal with the boundary conditions for these holes. Thus, we propose a topological derivative formulation for fluid flow channel design based on the concept of traditional topology optimization formulations in which solid or fluid material is distributed at each point of the domain to optimize the cost function subject to some constraints. By using this idea, the problem of dealing with the hole boundary conditions during the optimization process is solved because the asymptotic expansion is performed with respect to the nucleation of inclusions – which mimic solid or fluid phases – instead of inserting or removing holes in the fluid domain, which allows for working in a fixed computational domain. To evaluate the formulation, an optimization problem which consists in minimizing the energy dissipation in fluid flow channels is implemented. Results from considering Stokes and Navier-Stokes are presented and compared, as well as two- (2D) and three-dimensional (3D) designs. The topologies can be obtained in a few iterations with well defined boundaries.

1. Introduction

The application of topology optimization methods for viscous fluid flow problems is an active area of research. The objective of optimization is to distribute fluid or solid in a design domain to extremise a defined objective function subjected to some constraints. Following this way, we can find many works in the literature that apply topology optimization methods based on a material model definition to perform optimization of fluid flow channels. We can cite the work [12] who minimized the dissipated power in a flow channel by considering a 2D Brinkman medium. The flow modelling is restricted to the incompressible Stokes flow, and a porous flow model is introduced to relax the optimization problem from an integer (black–white) problem, in which either fluid or solid property is allowed in an element, to a continuous problem where a continuous (grey) permeability design variable for each element is defined. Thus, in the optimization problem, flow and (almost) non-flow regions are obtained by allowing interpolation schemes between the upper and lower values of the permeability [19, 20]. Some works have improved this formulation and implemented topology optimization approach in other flow conditions [12, 17, 18, 22, 33, 38]. Thus, for example, the topology optimization method is extended to full Navier-Stokes flow to cover from low to moderate Reynolds numbers into 2D domains in [19] and [21].

Another general approach to deal with shape and topology optimization design is based on the topological derivative. In fact, this relatively new concept represents the first term of the asymptotic expansion of a given shape functional with respect to the small parameter which measures the size of singular domain perturbations, such as holes, inclusions, source-terms and cracks. The topological asymptotic analysis was introduced in the fundamental paper [35] and has been successfully applied to the treatment of problems such as topology optimization [9], inverse analysis [27], image processing [26], multi-scale constitutive modeling [8], fracture mechanics sensitivity analysis [37] and damage evolution modeling [1]. For an account of new

Key words and phrases. topological derivative, fluid flow channel design, Stokes, Navier-Stokes, Darcy's law.

developments in this branch of shape optimization we refer to the book by Novotny & Sokołowski [31].

Alternatively to topological derivative and density-based approaches, we can mention the level set method, which has successfully been applied to the context of topology optimization of fluids in Stokes flow [14].

In this work, the topological derivative is applied in the context of topology optimization of steady-state fluid flow channels. A first work dealing with such a problem was published in [24]. In their work, the topological sensitivity analysis with respect to the insertion of a small hole or obstacle inside a domain has been used to perform the shape optimization considering Stokes equations. The paper [5] extends this work to Navier-Stokes equations by considering an incompressible fluid and a no-slip condition prescribed on the boundary of an arbitrary shaped obstacle. So far the implemented methods can only create small holes inside the domain. Once these holes have been created, they usually remain unchanged during the topological phase of the optimization algorithm. Thus, in [23] a new topological derivative method is introduced, which allows the decision of whether an existing hole must be removed or not for improving the cost function. In addition, in [11] a shape optimization problem with Stokes constraints within the class of axisymmetric domains is studied by using topological derivatives. Finally, in [16] the topological derivative is combined with standard level-set method for the optimal shape design of Stokes flow. For the theoretical development of shape and topology optimization in the context of compressible Navier-Stokes see, for instance, the book [34].

As mentioned, in these previous topological derivative works the topology is obtained by nucleating and/or removing holes in the fluid domain which creates numerical difficulties to deal with the boundary conditions in these holes. We thus, propose a topological derivative formulation for fluid flow channel design based on the concept of traditional topology optimization formulations where solid or fluid material is distributed in a porous medium to optimize the cost function and satisfy constraints. This is achieved by combining Stokes or Navier–Stokes equations with Darcy's law equations as first proposed in [12]. By using this idea, the problem of dealing with the hole boundary conditions in topological derivatives during the optimization process is solved. Note that holes can be interpreted as solid obstacles. Thus, inclusions mimicking solid or fluid phases are created, instead of inserting/removing holes, which allow for working in a fixed computational domain. Thus, the asymptotic expansion is performed with respect to the nucleation of inclusions instead of inserting or removing holes in the fluid domain (see Fig. 2). The theoretical results are then used to devise a topology design algorithm of remarkably simple computational implementation, which features only a minimal number of user-defined algorithmic parameters. To evaluate the formulation, an optimization problem which consists of minimizing the energy dissipation in fluid flow channels is implemented. Results considering Stokes and Navier-Stokes equations combined with Darcy's law equation are presented and compared, as well as two- (2D) and three-dimensional (3D) designs.

The paper is organized as follows. In Section 2, the topology optimization problem is defined. In Section 3 the topological asymptotic analysis of the energy shape functional associated with the Stokes system combined with Darcy's law equation is developed. In Section 4, the topological derivative with respect to the nucleation of a circular inclusion of the energy shape functional associated with the Navier-Stokes systems combined with Darcy's law equation is obtained in its closed form. In Section 5, the topology optimization algorithm is presented and in Section 6, its numerical implementation is discussed. In Section 7, some numerical experiments of topology optimization of fluid flow channels are presented. Finally, some concluding remarks and perspectives are inferred in Section 8.

2. Topology Optimization Problem

Let us consider an open and bounded domain $\Omega \subset \mathbb{R}^d$, $d \geq 2$, with Lipschitz continuous boundary $\partial\Omega$. The domain Ω is subjected to a perturbation confined in a small ball $B_\varepsilon(\widehat{x})$ of radius ε and center at an arbitrary point $\widehat{x}$ of Ω, namely $B_\varepsilon(\widehat{x}) := \{\|x - \widehat{x}\| < \varepsilon\}$, for $\widehat{x} \in \Omega$. We introduce a characteristic function $x \mapsto \chi(x)$, $x \in \mathbb{R}^d$, associated to the unperturbed

domain, namely $\chi = \mathbb{1}_\Omega$. Then, we define a characteristic function associated to the topologically perturbed domain of the form $x \mapsto \chi_\varepsilon(\widehat{x}; x)$, $x \in \mathbb{R}^d$. In the case of a hole, for example, $\chi_\varepsilon(\widehat{x}) = \mathbb{1}_\Omega - \mathbb{1}_{\overline{B_\varepsilon(\widehat{x})}}$ and the perturbed domain is given by $\Omega_\varepsilon(\widehat{x}) = \Omega \setminus \overline{B_\varepsilon(\widehat{x})}$, where $\overline{B_\varepsilon(\widehat{x})}$ denotes the closure of the domain of the inserted hole. Then, we assume that a given shape functional $j(\chi_\varepsilon(\widehat{x}))$, associated to the topologically perturbed domain, admits the following topological asymptotic expansion [31]

$$j(\chi_\varepsilon(\widehat{x})) = j(\chi) + f(\varepsilon) D_T j(\widehat{x}) + o(f(\varepsilon)) \,, \tag{2.1}$$

where $j(\chi)$ is the shape functional associated to the unperturbed domain and $f(\varepsilon)$ is a positive function such that $f(\varepsilon) \to 0$ when $\varepsilon \to 0$. The function $\widehat{x} \mapsto D_T j(\widehat{x})$ is called the topological derivative of j at $\widehat{x}$. Therefore, the term $f(\varepsilon) D_T j(\widehat{x})$ represents a first order correction of $j(\chi)$ to approximate $j(\chi_\varepsilon(\widehat{x}))$.

2.1. **A Simple Example.** The notion of topological derivative extends the conventional definition of derivative to functionals whose variable is a *geometrical domain* subjected to singular topology changes. The analogy between $D_T j(\widehat{x})$ and the corresponding expressions for a conventional derivative should be noted. To illustrate the application of this concept, let us consider the (very simple) functional

$$j(\chi) := |\Omega| = \int_\Omega 1, \tag{2.2}$$

with $\Omega \subset \mathbb{R}^2$ subject to the class of topological perturbations given by the nucleation of circular holes. See Fig. 1. For two-dimensional domains Ω the functional $j(\chi)$ represents the area of the domain. The expansion of (2.1) in this case can be obtained trivially as

$$j(\chi_\varepsilon) = |\Omega_\varepsilon| = \int_\Omega 1 - \int_{B_\varepsilon} 1 = j(\chi) - \pi\varepsilon^2, \tag{2.3}$$

and the topological derivative $D_T j(\widehat{x})$ and function $f(\varepsilon)$ promptly identified as

$$D_T j(\widehat{x}) = -1; \qquad f(\varepsilon) = \pi\varepsilon^2. \tag{2.4}$$

In this particular case, $D_T j$ is independent of $\widehat{x}$ and the rightmost term of the topological asymptotic expansion (2.1) is equal to zero.

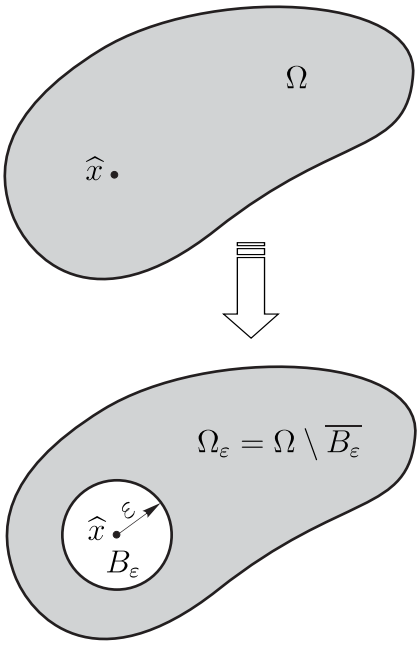

FIGURE 1. An example of topological domain perturbation.

2.2. **Problem Setting.** Now, considering the fluid flow channel design problem the energy shape functional can be introduced in the form

$$j(\chi) := \mathcal{J}(u) = \mu \int_\Omega \|\nabla u\|^2 + \int_\Omega \alpha \|u\|^2 \,, \tag{2.5}$$

where $0 < \mu < \infty$ is the kinematic viscosity, α is the inverse permeability and u is the solution to the unperturbed fluid flow problems (3.2) or (4.2). The topological perturbation we are dealing with is defined as

$$\gamma_\varepsilon = \gamma_\varepsilon(x) := \left\{ \begin{array}{ll} 1 & \text{if } x \in \Omega \setminus \overline{B_\varepsilon} \,, \\ \gamma & \text{if } x \in B_\varepsilon \,, \end{array} \right. \tag{2.6}$$

where $0 < \gamma < \infty$ is the contrast parameter and $B_\varepsilon(\widehat{x})$ is a ball of radius ε and center at $\widehat{x} \in \Omega$. The topologically perturbed counterpart of the inverse permeability is obtained by setting $\alpha_\varepsilon = \gamma_\varepsilon \alpha$. Therefore, the topologically perturbed energy shape functional is given by

$$j(\chi_\varepsilon(\widehat{x})) := \mathcal{J}_\varepsilon(u_\varepsilon) = \mu \int_\Omega \|\nabla u_\varepsilon\|^2 + \int_\Omega \alpha_\varepsilon \|u_\varepsilon\|^2 \,, \tag{2.7}$$

where u_ε is solution to the topologically perturbed fluid flow problems (3.6) or (4.8). Now, let us split the domain Ω into two subdomains $\Omega \setminus \overline{\omega}$ and ω, with $\omega \subset \Omega$. The inverse permeability $\alpha = \alpha(x)$ is written as

$$\alpha(x) := \left\{ \begin{array}{ll} \alpha_U & \text{if } x \in \Omega \setminus \overline{\omega} \,, \\ \alpha_L & \text{if } x \in \omega \,, \end{array} \right. \tag{2.8}$$

where α_U and α_L are the upper and lower limits for the inverse permeability. Therefore, $\Omega \setminus \overline{\omega}$ and ω are used to represent the solid and fluid phases, respectively. To distribute solid and fluid, the topological derivative formulation does not use a material model concept such as in the topology optimization formulation based on density methods. Thus, the fact that we are not using an interpolation scheme for α eliminates the gray scale from the problem, i.e. there is no domain with intermediate porosities. Concerning the values of α_U and α_L, we refer to the paper [12]. According to (2.8), the contrast γ is defined as follows (refer to Fig. 2)

$$\gamma = \gamma(x) := \left\{ \begin{array}{ll} \alpha_L/\alpha_U & \text{if } x \in \Omega \setminus \overline{\omega} \,, \\ \alpha_U/\alpha_L & \text{if } x \in \omega \,. \end{array} \right. \tag{2.9}$$

Now, we introduce a volume constraint in ω of the form $|\omega| \leq M$. For the sake of simplicity, the volume constraint is here trivially imposed by using a linear penalization method. For more sophisticated topological derivative-based methods to deal with the volume constraint see, for instance, [13]. Therefore, the optimization problem we are dealing with can be written as follows:

$$\underset{\omega \subset \Omega}{\text{Minimize}}\ \mathcal{F}_\omega(u) = \mathcal{J}(u) + \beta |\omega| \,, \tag{2.10}$$

where β is a fixed multiplier. The topological derivative of the volume constraint is trivial, which is given by $D_T|\omega|(x) = k(x)$, where

$$k(x) := \left\{ \begin{array}{ll} +1 & \text{if } x \in \Omega \setminus \overline{\omega} \,, \\ -1 & \text{if } x \in \omega \,, \end{array} \right. \tag{2.11}$$

with function $f(\varepsilon) = |B_\varepsilon|$ and null remainder. Yet, the derivation of the topological derivative of the energy shape functional $\mathcal{J}(u)$ is much more involved and will be presented for each problem under analysis in what follows. The case associated to singular domain perturbations can be found in [5], in which the topological derivative with respect to the nucleation of a small hole endowed with homogeneous Dirichlet boundary condition has been rigorously derived for the Navier-Stokes system.

The Stokes problem is considered first to show a rigorous mathematical formalism for deriving the topological derivative. Then the same procedure is repeated in the derivation of the topological derivative associated with the Navier-Stokes system, however without mathematical proofs. The well-posedness of both Stokes and Navier-Stokes systems comes out from an application of the Lax-Milgram Lemma. See, for instance, [36, App. 1, pp 458]. Finally, the consistency of the topological derivatives formulae obtained is verified through some numerical experiments.

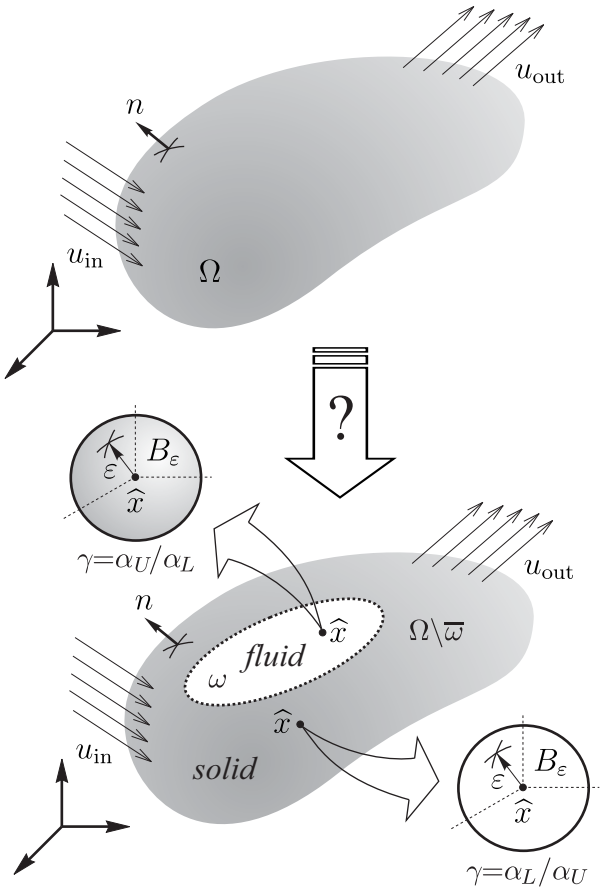

FIGURE 2. Sketch of the problem setting.

3. Topological Derivative for the Stokes System

In this section the topological asymptotic analysis of the energy shape functional associated with the Stokes system combined with Darcy's law equation is developed. The topological derivative with respect to the nucleation of a circular inclusion is derived in its closed form. In addition, a complete mathematical justification for the derived formula is provided. In particular, arguments concerning the existence of the associated topological derivative are presented together with the estimates for the remainders of the topological asymptotic expansion.

3.1. **Unperturbed Problem.** The Stokes system combined with Darcy's law equation reads: Find u and p, such that [12]

$$\left\{\begin{array}{rcll} -\mu\Delta u + \alpha u + \nabla p &=& 0 \quad \text{in} \quad \Omega\,, \\ \text{div}(u) &=& 0 \quad \text{in} \quad \Omega\,, \\ u &=& u_0 \quad \text{on} \quad \partial\Omega\,, \end{array}\right. \tag{3.1}$$

where $u_0 \in H^{1/2}(\Omega;\mathbb{R}^d) : \int_{\partial\Omega} u_0 \cdot \nu = 0$, with ν used to denote the outward unit normal of the boundary $\partial\Omega$. Thus, when the inverse permeability is equal to 0 the point is made of fluid and when it is equal to a maximum value the point is made of solid. The weak form associated with (3.1) reads:

$$u \in \mathcal{U} \;:\; \mu \int_\Omega \nabla u \cdot \nabla v + \int_\Omega \alpha u \cdot v = 0 \quad \forall v \in \mathcal{V}\,, \tag{3.2}$$

where $\mathcal{U}$ and $\mathcal{V}$ are given by

$$\mathcal{U} \;=\; \{\varphi \in H^1(\Omega;\mathbb{R}^d) : \text{div}(\varphi) = 0,\ \varphi_{|\partial\Omega} = u_0\}\,, \tag{3.3}$$

$$\mathcal{V} \;=\; \{\varphi \in H^1(\Omega;\mathbb{R}^d) : \text{div}(\varphi) = 0,\ \varphi_{|\partial\Omega} = 0\}\,, \tag{3.4}$$

The energy shape functional is given by (2.5).

3.2. **Perturbed Problem.** The topologically perturbed counterpart of the Stokes system reads: Find u_ε and p_ε, such that

$$\left\{\begin{array}{rcll} -\mu\Delta u_\varepsilon + \alpha_\varepsilon u_\varepsilon + \nabla p_\varepsilon &=& 0 \quad \text{in} \quad \Omega\,, \\ \operatorname{div}(u_\varepsilon) &=& 0 \quad \text{in} \quad \Omega\,, \\ u_\varepsilon &=& u_0 \quad \text{on} \quad \partial\Omega\,. \end{array}\right. \tag{3.5}$$

The weak form associated with (3.5) reads:

$$u_\varepsilon \in \mathcal{U} \;:\; \mu\int_\Omega \nabla u_\varepsilon\cdot\nabla v + \int_\Omega \alpha_\varepsilon u_\varepsilon\cdot v = 0 \quad \forall v\in\mathcal{V}\,, \tag{3.6}$$

The topologically perturbed counterpart of the shape functional is given by (2.7).

Lemma 1. *Let u_ε and u be solutions to the perturbed* (3.6) *and original* (3.2) *variational problems, respectively. Then, the following estimate holds true*

$$\|u_\varepsilon - u\|_{H^1(\Omega;\mathbb{R}^d)} \leq C\varepsilon^{\frac{d}{2}+\delta}\,. \tag{3.7}$$

where $0<\delta\leq 1$ and C is used to denote a generic constant independent of control parameter ε.

Proof. By subtracting (3.2) from (3.6), we have:

$$\mu\int_\Omega \nabla(u_\varepsilon - u)\cdot\nabla v + \int_\Omega (\alpha_\varepsilon u_\varepsilon - \alpha u)\cdot v = 0\;\forall v\in\mathcal{V}\,. \tag{3.8}$$

Let us set $v = u_\varepsilon - u$ as a test function in (3.8). Then

$$\mu\int_\Omega \|\nabla(u_\varepsilon - u)\|^2 + \int_\Omega (\alpha_\varepsilon u_\varepsilon - \alpha u)\cdot(u_\varepsilon - u) = 0. \tag{3.9}$$

From the definition of the contrast γ_ε given by (2.6), the second term in the above equation can be written as

$$\int_\Omega (\alpha_\varepsilon u_\varepsilon - \alpha u)\cdot(u_\varepsilon - u) = \int_{\Omega\setminus\overline{B_\varepsilon}} \alpha\|u_\varepsilon - u\|^2 + \int_{B_\varepsilon} \alpha(\gamma u_\varepsilon - u)\cdot(u_\varepsilon - u)\,, \tag{3.10}$$

since $\alpha_\varepsilon = \gamma_\varepsilon\alpha$. In addition, using again definition (2.6), we obtain

$$\int_\Omega (\alpha_\varepsilon u_\varepsilon - \alpha u)\cdot(u_\varepsilon - u) = \int_\Omega \alpha_\varepsilon\|u_\varepsilon - u\|^2 - \int_{B_\varepsilon} (1-\gamma)\alpha u\cdot(u_\varepsilon - u)\,. \tag{3.11}$$

Therefore, eq. (3.9) can be rewritten as

$$\mu\int_\Omega \|\nabla(u_\varepsilon - u)\|^2 + \int_\Omega \alpha_\varepsilon\|u_\varepsilon - u\|^2 = \int_{B_\varepsilon} (1-\gamma)\alpha u\cdot(u_\varepsilon - u)\,. \tag{3.12}$$

Taking into account the Cauchy-Schwarz inequality and the Lebesgue differentiation theorem [28], we have:

$$\mu\int_\Omega \|\nabla(u_\varepsilon - u)\|^2 + \int_\Omega \alpha_\varepsilon\|u_\varepsilon - u\|^2 \leq C_1\varepsilon^{\frac{d}{2}}\,\|u_\varepsilon - u\|_{L^2(B_\varepsilon;\mathbb{R}^d)}\,. \tag{3.13}$$

In addition, by making use of the Hölder inequality together with the Sobolev embedding theorem [15, Ch. IV, §8, Sec. 1.2, pp 140], we have

$$\begin{aligned} \|u_\varepsilon - u\|_{L^2(B_\varepsilon;\mathbb{R}^d)} &\leq C_2\varepsilon^{\frac{d}{2q}}\left(\int_{B_\varepsilon}\|u_\varepsilon - u\|^{2p}\right)^{\frac{1}{2p}} \\ &= C_2\varepsilon^{\frac{d}{2q}}\|u_\varepsilon - u\|_{L^{2p}(B_\varepsilon;\mathbb{R}^d)} \\ &\leq C_3\varepsilon^{\delta}\|u_\varepsilon - u\|_{H^1(\Omega;\mathbb{R}^d)}\,, \end{aligned} \tag{3.14}$$

where $1/p + 1/q = 1$, with $q\geq d/2$, and $\delta = d/2q$. Therefore,

$$\mu\int_\Omega \|\nabla(u_\varepsilon - u)\|^2 + \int_\Omega \alpha_\varepsilon\|u_\varepsilon - u\|^2 \leq C_4\varepsilon^{\frac{d}{2}+\delta}\,\|u_\varepsilon - u\|_{H^1(\Omega;\mathbb{R}^d)}\,. \tag{3.15}$$

From the coercivity of the bilinear form on the left hand side of the above inequality, we obtain

$$c\|u_\varepsilon - u\|^2_{H^1(\Omega;\mathbb{R}^d)} \leq \mu \int_\Omega \|\nabla(u_\varepsilon - u)\|^2 + \int_\Omega \alpha_\varepsilon \|u_\varepsilon - u\|^2 \,, \tag{3.16}$$

where the constant $C = C_4/c$ is independent of the small parameter ε. □

3.3. **Topological Derivative.** By setting $v = u_\varepsilon - u$ in (3.2) and (3.6) and after taking into account (2.5) and (2.7), we respectively obtain

$$\mathcal{J}(u) = \mu \int_\Omega \nabla u_\varepsilon \cdot \nabla u + \int_\Omega \alpha u_\varepsilon \cdot u \,, \tag{3.17}$$

and

$$\mathcal{J}_\varepsilon(u_\varepsilon) = \mu \int_\Omega \nabla u_\varepsilon \cdot \nabla u + \int_\Omega \alpha_\varepsilon u_\varepsilon \cdot u \,. \tag{3.18}$$

Let us evaluate the difference between the above results. Then, from the definition of the contrast γ_ε in (2.6), we have

$$\begin{aligned} \mathcal{J}_\varepsilon(u_\varepsilon) - \mathcal{J}(u) &= -\int_{B_\varepsilon} (1-\gamma)\alpha u_\varepsilon \cdot u \\ &= -\int_{B_\varepsilon} (1-\gamma)\alpha \|u\|^2 \\ &\quad -\int_{B_\varepsilon} (1-\gamma)\alpha (u_\varepsilon - u)\cdot u \,. \end{aligned} \tag{3.19}$$

From the Cauchy-Schwarz inequality we have

$$\begin{aligned} \int_{B_\varepsilon} \alpha(u_\varepsilon - u)\cdot u &\leq C_1 \varepsilon^{\frac{d}{2}} \, \|u_\varepsilon - u\|_{L^2(B_\varepsilon;\mathbb{R}^d)} \\ &\leq C_2 \varepsilon^{\frac{d}{2}} \, \|u_\varepsilon - u\|_{H^1(\Omega;\mathbb{R}^d)} = o(\varepsilon^d) \,. \end{aligned} \tag{3.20}$$

where we have used the Lebesgue differentiation theorem [28] together with Lemma 1. Finally,

$$\mathcal{J}_\varepsilon(u_\varepsilon) - \mathcal{J}(u) = -\int_{B_\varepsilon} (1-\gamma)\alpha\|u\|^2 + o(\varepsilon^d) \,. \tag{3.21}$$

On the other hand, the Lebesgue differentiation theorem yields

$$\int_{B_\varepsilon} (1-\gamma)\alpha\|u\|^2 = |B_\varepsilon(\widehat{x})| \, (1-\gamma(\widehat{x}))\alpha(\widehat{x}) \, \|u(\widehat{x})\|^2 + o(\varepsilon^d) \,, \tag{3.22}$$

for almost every $\widehat{x} \in \Omega$. Now, we have all the necessary elements to state the main result of this work, which is:

Theorem 2. *Let $\mathcal{J}_\varepsilon(u_\varepsilon)$ be the topologically perturbed shape function (2.7). Then, it admits the following topological asymptotic expansion*

$$\mathcal{J}_\varepsilon(u_\varepsilon) = \mathcal{J}(u) - |B_\varepsilon(\widehat{x})|(1-\gamma(\widehat{x}))\alpha(\widehat{x})\|u(\widehat{x})\|^2 + o(\varepsilon^d) \,, \tag{3.23}$$

for almost every $\widehat{x} \in \Omega$. According to (2.1), the function $f(\varepsilon) = |B_\varepsilon(\widehat{x})| \sim \varepsilon^d$ and the topological derivative is given by

$$D_T\mathcal{J}(\widehat{x}) = -(1-\gamma(\widehat{x}))\alpha(\widehat{x})\|u(\widehat{x})\|^2 \,, \tag{3.24}$$

where α is given by (2.8) and u is the solution to the unperturbed problem (3.2).

Corollary 3. *By setting the contrast γ according to (2.9), the topological derivative of $\mathcal{F}_\omega(u)$ associated with the Stokes system leads to*

$$D_T\mathcal{F}_\omega(x) = -k(x)(\alpha_U - \alpha_L)\|u(x)\|^2 + k(x)\beta \,, \tag{3.25}$$

for almost every $x \in \Omega$. Here, $\alpha_U \gg \alpha_L$ are given constants and $k(x)$ is defined by (2.11). Finally, u is the solution to the unperturbed problem (3.2).

4. Topological Derivative of the Navier-Stokes System

In this section the topological derivative with respect to the nucleation of a circular inclusion of the energy shape functional associated with the Navier-Stokes systems combined with Darcy's law is obtained in its closed form. In contrast to the Stokes system, only the formal derivations are presented.

4.1. **Unperturbed Problem.** The Navier-Stokes system combined with Darcy's law equation reads: Find u and p, such that

$$\left\{\begin{array}{rcll} -\mu\Delta u + (\nabla u)u + \alpha u + \nabla p &=& 0 \quad \text{in} \quad \Omega\,, \\ \operatorname{div}(u) &=& 0 \quad \text{in} \quad \Omega\,, \\ u &=& u_0 \quad \text{on} \quad \partial\Omega\,, \end{array}\right. \tag{4.1}$$

where $u_0 \in H^{1/2}(\Omega;\mathbb{R}^d) : \int_{\partial\Omega} u_0 \cdot \nu = 0$, with ν denoting the outward unit normal of the boundary $\partial\Omega$. Thus, again, when the inverse permeability is equal to 0 the point is made of fluid and when it is equal to a maximum value the point is made of solid. The weak form associated with (4.1) reads:

$$u \in \mathcal{U} \;:\; \mu\int_\Omega \nabla u \cdot \nabla v + \int_\Omega (\nabla u)u \cdot v + \int_\Omega \alpha u \cdot v = 0 \quad \forall v \in \mathcal{V}\,, \tag{4.2}$$

where $\mathcal{U}$ and $\mathcal{V}$ are given by

$$\mathcal{U} = \{\varphi \in H^1(\Omega;\mathbb{R}^d) : \operatorname{div}(\varphi) = 0,\ \varphi_{|\partial\Omega} = u_0\}\,, \tag{4.3}$$

$$\mathcal{V} = \{\varphi \in H^1(\Omega;\mathbb{R}^d) : \operatorname{div}(\varphi) = 0,\ \varphi_{|\partial\Omega} = 0\}\,. \tag{4.4}$$

The energy shape functional is defined by (2.5). In order to simplify further analysis, we introduce the adjoint problem [25]: Find u^a and p^a, such that

$$\left\{\begin{array}{rcll} -\mu\Delta u^a + (\nabla u)^\top u^a - (\nabla u^a)u + \alpha u^a + \nabla p^a &=& 2(\alpha u - \mu\Delta u) \quad \text{in} \quad \Omega\,, \\ \operatorname{div}(u^a) &=& 0 \quad \text{in} \quad \Omega\,, \\ u^a &=& 0 \quad \text{on} \quad \partial\Omega\,. \end{array}\right. \tag{4.5}$$

The weak form associated with (4.5) reads:

$$u^a \in \mathcal{V} \;:\; \mu\int_\Omega \nabla u^a \cdot \nabla v + \int_\Omega ((\nabla u)^\top u^a - (\nabla u^a)u) \cdot v + \int_\Omega \alpha u^a \cdot v = 2\mu\int_\Omega \nabla u \cdot \nabla v + 2\int_\Omega \alpha u \cdot v \quad \forall v \in \mathcal{V}\,, \tag{4.6}$$

4.2. **Perturbed Problem.** The topologically perturbed counterpart of the Navier-Stokes system combined with Darcy's law equation reads: Find u_ε and p_ε, such that

$$\left\{\begin{array}{rcll} -\mu\Delta u_\varepsilon + (\nabla u_\varepsilon)u_\varepsilon + \alpha_\varepsilon u_\varepsilon + \nabla p_\varepsilon &=& 0 \quad \text{in} \quad \Omega\,, \\ \operatorname{div}(u_\varepsilon) &=& 0 \quad \text{in} \quad \Omega\,, \\ u_\varepsilon &=& u_0 \quad \text{on} \quad \partial\Omega\,. \end{array}\right. \tag{4.7}$$

The weak form associated with (4.7) reads:

$$u_\varepsilon \in \mathcal{U} \;:\; \mu\int_\Omega \nabla u_\varepsilon \cdot \nabla v + \int_\Omega (\nabla u_\varepsilon)u_\varepsilon \cdot v + \int_\Omega \alpha_\varepsilon u_\varepsilon \cdot v = 0 \quad \forall v \in \mathcal{V}\,, \tag{4.8}$$

The topologically perturbed counterpart of the shape functional is given by (2.7).

4.3. **Topological Derivative.** From the definition of the contrast (2.6), the difference between the unperturbed and topologically perturbed shape functionals, respectively given by (2.5) and (2.7), can be written in the following form

$$\mathcal{J}_\varepsilon(u_\varepsilon) - \mathcal{J}(u) = 2\mu\int_\Omega \nabla u \cdot \nabla(u_\varepsilon - u) + 2\int_\Omega \alpha u \cdot (u_\varepsilon - u) + \mu\int_\Omega \|\nabla(u_\varepsilon - u)\|^2 + \int_\Omega \alpha_\varepsilon \|u_\varepsilon - u\|^2 + 2\int_{B_\varepsilon} (1-\gamma)\alpha u \cdot (u_\varepsilon - u) - \int_{B_\varepsilon} (1-\gamma)\alpha\|u\|^2\,. \tag{4.9}$$

By subtracting (4.2) from (4.8), we have:

$$\mu\int_\Omega \nabla(u_\varepsilon-u)\cdot\nabla v+\int_\Omega((\nabla u_\varepsilon)u_\varepsilon-(\nabla u)u)\cdot v+\int_\Omega \alpha(u_\varepsilon-u)\cdot v- \int_{B_\varepsilon}(1-\gamma)\alpha u_\varepsilon\cdot v=0 \quad \forall v\in\mathcal{V}\,, \tag{4.10}$$

where we have used the definition for the contrast (2.6). From the integration by parts we have

$$\mu\int_\Omega \nabla(u_\varepsilon-u)\cdot\nabla v+\int_\Omega((\nabla u)^\top v-(\nabla v)u)\cdot(u_\varepsilon-u)+\int_\Omega \alpha(u_\varepsilon-u)\cdot v+ \int_\Omega(\nabla(u_\varepsilon-u))(u_\varepsilon-u)\cdot v-\int_{B_\varepsilon}(1-\gamma)\alpha u_\varepsilon\cdot v=0 \quad \forall v\in\mathcal{V}\,. \tag{4.11}$$

By setting $v=u^a$ in the above equation, we obtain the equality

$$\mu\int_\Omega \nabla(u_\varepsilon-u)\cdot\nabla u^a+\int_\Omega((\nabla u)^\top u^a-(\nabla u^a)u)\cdot(u_\varepsilon-u)+\int_\Omega \alpha(u_\varepsilon-u)\cdot u^a= \int_{B_\varepsilon}(1-\gamma)\alpha u_\varepsilon\cdot u^a-\int_\Omega(\nabla(u_\varepsilon-u))(u_\varepsilon-u)\cdot u^a\,. \tag{4.12}$$

Now, let us set $v=u_\varepsilon-u$ in the adjoint equation (4.6). Then, we obtain the following equality

$$\mu\int_\Omega \nabla u^a\cdot\nabla(u_\varepsilon-u)+\int_\Omega((\nabla u)^\top u^a-(\nabla u^a)u)\cdot(u_\varepsilon-u)+\int_\Omega \alpha u^a\cdot(u_\varepsilon-u)= 2\mu\int_\Omega \nabla u\cdot\nabla(u_\varepsilon-u)+2\int_\Omega \alpha u\cdot(u_\varepsilon-u)\,, \tag{4.13}$$

After comparing (4.12) with (4.13) we obtain the following important result

$$2\mu\int_\Omega \nabla u\cdot\nabla(u_\varepsilon-u)+2\int_\Omega \alpha u\cdot(u_\varepsilon-u)= \int_{B_\varepsilon}(1-\gamma)\alpha u_\varepsilon\cdot u^a-\int_\Omega(\nabla(u_\varepsilon-u))(u_\varepsilon-u)\cdot u^a\,. \tag{4.14}$$

Finally, let us substitute this last result in (4.9) to obtain

$$\mathcal{J}_\varepsilon(u_\varepsilon)-\mathcal{J}(u)=-\int_{B_\varepsilon}(1-\gamma)\alpha u\cdot(u-u^a)+\mathcal{E}(\varepsilon), \tag{4.15}$$

where $\mathcal{E}(\varepsilon)$ is given by

$$\mathcal{E}(\varepsilon)=\mu\int_\Omega\|\nabla(u_\varepsilon-u)\|^2+\int_\Omega\alpha_\varepsilon\|u_\varepsilon-u\|^2-\int_\Omega(\nabla(u_\varepsilon-u))(u_\varepsilon-u)\cdot u^a+ \int_{B_\varepsilon}(1-\gamma)\alpha u^a\cdot(u_\varepsilon-u)-2\int_{B_\varepsilon}(1-\gamma)\alpha u\cdot(u_\varepsilon-u)\,. \tag{4.16}$$

Now, from the Lebesgue differentiation theorem [28] we finally obtain

$$\mathcal{J}_\varepsilon(u_\varepsilon)\approx\mathcal{J}(u)-|B_\varepsilon(\widehat{x})|(1-\gamma(\widehat{x}))\alpha(\widehat{x})u(\widehat{x})\cdot(u(\widehat{x})+u^a(\widehat{x}))\,, \tag{4.17}$$

for almost every $\widehat{x}\in\Omega$. According to (2.1), the function $f(\varepsilon)=|B_\varepsilon(\widehat{x})|\sim\varepsilon^d$ and the topological derivative is given by

$$D_T\mathcal{J}(\widehat{x})=-(1-\gamma(\widehat{x}))\alpha(\widehat{x})u(\widehat{x})\cdot(u(\widehat{x})-u^a(\widehat{x}))\,, \tag{4.18}$$

where α is defined through (2.8). In addition, u is the solution of the direct problem (4.2) and u^a is solution of the adjoint problem (4.6), both associated with the unperturbed domain Ω. Finally, by setting the contrast γ according to (2.9), the topological derivative of $\mathcal{F}_\omega(u)$ associated to the Navier-Stokes system combined with Darcy's law equation leads to

$$D_T\mathcal{F}_\omega(x)=-k(x)(\alpha_U-\alpha_L)u(x)\cdot(u(x)-u^a(x))+k(x)\beta, \tag{4.19}$$

for almost every $x \in \Omega$, where $\alpha_U \gg \alpha_L$ are given constants and $k(x)$ is defined through (2.11). In addition, u and u^a are solutions of the direct (4.2) and adjoint (4.6) unperturbed problems, respectively.

5. Topology Optimization Algorithm

The topological derivative is defined through a limit passage when the small parameter governing the size of the topological perturbation goes to zero. Therefore, it can be used as a steepest-descent direction in an optimization process such as in any method based on the gradient of the cost functional. Thus, following the original ideas due to Amstutz & Andrä [7], the results given by (3.25) and (4.19) are used to devise a topology optimization algorithm based on the topological derivative together with a level-set domain representation method. For the sake of completeness, the algorithm for the solution of the topology optimization problem proposed in [7] is presented. The basic idea consists in seeking a local optimality condition for the minimization problem (2.10), written in terms of the topological derivative and a level-set function. Such a *local optimality condition* has been rigorously derived in [6]. Therefore, fluid ω as well as solid $\Omega \setminus \overline{\omega}$ are characterized by a level-set function $\psi \in L^2(\Omega)$ of the form:

$$\omega = \{\psi(x) < 0, \text{ for } x \in \Omega\}, \tag{5.1}$$

$$\Omega \setminus \overline{\omega} = \{\psi(x) > 0, \text{ for } x \in \Omega\}, \tag{5.2}$$

where ψ vanishes in interface $\partial\omega$. A locally sufficient optimality condition for Problem (2.10), under the considered class of domain perturbation given by circular inclusions, can be stated as [6]

$$D_T\mathcal{F}_{\omega^\star}(x) > 0 \quad \forall x \in \Omega\,. \tag{5.3}$$

where $\omega^\star$ is a local minimum for Problem (2.10). Therefore, let us define the quantity

$$g(x) := \begin{cases} -D_T\mathcal{F}_\omega(x), & \text{if } \psi(x) < 0\,, \\ +D_T\mathcal{F}_\omega(x), & \text{if } \psi(x) > 0\,. \end{cases} \tag{5.4}$$

allowing for rewriting the condition (5.3) in the following equivalent form

$$\begin{cases} g(x) < 0, & \text{if } \psi(x) < 0, \\ g(x) > 0, & \text{if } \psi(x) > 0. \end{cases} \tag{5.5}$$

Note that (5.5) is satisfied whenever quantity g coincides with level-set function ψ up to a strictly positive number, namely $\exists\, \tau > 0 : g = \tau\psi$, or equivalently [6]

$$\theta := \arccos\left[\frac{\langle g, \psi\rangle_{L^2(\Omega)}}{\|g\|_{L^2(\Omega)}\|\psi\|_{L^2(\Omega)}}\right] = 0, \tag{5.6}$$

which shall be used as the optimality condition in the topology design algorithm, where θ is the angle between the functions g and ψ in $L^2(\Omega)$.

Let us now explain the algorithm. We start by choosing an initial level-set function $\psi_0 \in L^2(\Omega)$. In a generic iteration n, we compute function g_n associated with the level-set function $\psi_n \in L^2(\Omega)$. In order to evaluate g_n, two cases are considered according to eqs. (3.25) or (4.19), respectively. For the Stokes problem, it is necessary to solve only (3.2) to obtain u_n associated with ψ_n. Whereas, for the Navier-Stokes problem, it is necessary to solve (4.2) and then the corresponding adjoint system (4.6) to obtain u_n and u_n^a, both associated with ψ_n. Thus, the new level-set function ψ_{n+1} is updated according to the following linear combination between the functions g_n and ψ_n

$$\psi_0 \in L^2(\Omega)\,, \quad \psi_{n+1} = \frac{1}{\sin\theta_n}\left[\sin((1-\kappa)\theta_n)\psi_n + \sin(\kappa\theta_n)\frac{g_n}{\|g_n\|_{L^2(\Omega)}}\right], \quad \forall n \in \mathbb{N}, \tag{5.7}$$

where θ_n is the angle between g_n and ψ_n. Step size κ is determined by a line search performed in order to decrease the value of the objective function $\mathcal{F}_{\omega_n}(u_n) = \mathcal{J}(u_n) + \beta|\omega_n|$ associated with ψ_n, where ω_n is used to denote the region in Ω filled by the fluid at iteration n. Since the shape functional depends on the state, the governing Stokes or Navier–Stokes systems have to

be solved at each step of the internal loop associated with the line search procedure. In any case, we observe that the step size parameter κ generally starts to diminish only at the end of the iterative process, close to the convergence. Furthermore, since in this case an analytical – *exact* – expression for the topological sensitivity is available, the number of iterations to obtain the optimized solution is here drastically reduced. Finally, the algorithm ends when the condition $\theta_n \leq \epsilon_\theta$ is satisfied in some iteration, where ϵ_θ is a given small numerical tolerance. Particularly, we can choose

$$\psi_0 \in \mathcal{S} = \{\varphi \in L^2(\Omega) : \|\varphi\|_{L^2(\Omega)} = 1\}, \tag{5.8}$$

and by construction $\psi_{n+1} \in \mathcal{S}$, $\forall n \in \mathbb{N}$. If at some iteration n the line search step size κ is found to be smaller then a given numerical tolerance $\epsilon_\kappa > 0$ and the optimality condition is not satisfied, namely $\theta_n > \epsilon_\theta$, a uniform mesh refinement of the whole domain Ω is carried out and the iterative process is continued.

However, current, the algorithm solves the governing equations (Stokes or Navier-Stokes) every function evaluation which is not so efficient if a nonlinear governing equation (such as Navier-Stokes) is considered. This limits the application of this algorithm for large computational problems. Thus, as a future work, it can be implemented a onestep approach where the governing equations and line search would be solved simultaneously [32, 18].

6. Numerical Implementation

The FEniCS environment and its Python interface are used herein. The FEniCS system [30] is a free collection of software components for automating the solution of PDEs by using the finite element method. It has as input the weak formulation of the problem, in a language very similar to the math syntax. It is thus, necessary to use a software capable of interpreting this high-level language and to transform it into a numerical routine. This interpretation software is the FEniCS Form Compiler (FFC), that receives a discrete form of the weak variational equation given in Unified Form Language (UFL) [2], similar to the mathematical formulation, and generates a C++ code of the finite element assembly in the format of the Unified Form-Assembly Code (UFC) [3]. This assembly is an optimised low-level code that evaluates the local element tensors.

The local tensors are used by DOLFIN [29], a library that handles the communication between all the FEniCS modules. This library also provides various data structures to interface meshes, function spaces, functions and solvers. The FEniCS environment allows using many linear algebra, such as PETSc used in this work.

To solve the Navier-Stokes problem, the FEniCS system offers pre-installed support to methods such as Generalized Minimal RESidual (GMRES). However, some external solvers can be used, and the MUltifrontal Massively Parallel Sparse direct solver (MUMPS) [4] was chosen here because it offers features such as input of the matrix in assembled format (distributed or centralized), error analysis and parallel analysis.

To illustrate how user-friendly the FEniCS API is, a small example of the implementation for the Navier-Stokes system is shown below.

```
F = (
    #Momentum
      mu * inner( grad(u), grad(v) ) * dx \
      + inner( grad(u) * u, v ) * dx \
      + alpha * inner( u, v ) * dx \
      - p * div( v ) * dx

    #Continuity
      + q*div(u)*dx \
)
```

Listing 1. Variational problem in FEniCS notation

7. Numerical Experiments

Five implementation examples are presented in this section. In all of them, the fluid density is set as $\rho = 1.0$ while the kinematic viscosity μ varies for each example. According to the paper [12], the inverse permeability α is set as $\alpha_U = 2.5\mu/100^2$ and $\alpha_L = 2.5\mu/0.01^2$ for all the examples. Note that the limit cases $\alpha_L \to 0$ and $\alpha_U \to \infty$ have to be justified. Since it is out of the scope of this work, we refer to the paper [10], where these limit cases are discussed together with the concept of degenerated topological derivative. The Reynolds number $Re = uL/\mu$ is obtained by considering the inlet length and inlet radius as characteristic length (L), for 2D and 3D examples, respectively. For cases with two inlets, only the length (or radius) of one inlet is considered. In the figures, the fluid domain is represented by an orange path whereas the solid domain is represented by a blue path. Finally, the thresholds for the external topology optimization and internal line search loops, described in the algorithm of Section 5, are respectively given by $\epsilon_\theta = 0.1°$ and $\epsilon_\kappa = 10^{-4}$. These parameters were fixed after some trials allowing to represent a good compromise between the quality of the results and the computational cost.

The results presented in the following sections were computed with a Linux machine with an Intel Core i7 (3.7GHz) processor and 64Gb of memory.

7.1. **Example 1: Stokes Short and Long Double Channel Problems.** The first implementation example is the Stokes double channel optimization problem. The corresponding design domain is shown in Figure 3. The objective is the minimization of energy dissipation between inlets and outlets. In the following results, the domain is discretized with a regular mesh of 45,000 triangular elements during the optimization procedure.

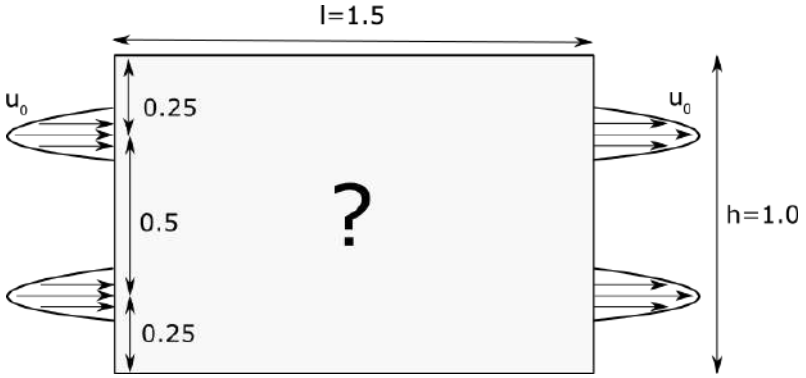

Figure 3. Example 1. Design domain for the double channel problem.

As a result, a comparison of topologies generated by considering Stokes equations is presented for the short ($l = 1.0$) and long ($l = 1.5$) channels for low values of Reynolds number ($Re = 0.2$, $u_0 = 1.0$). The value of the β coefficient is equal to 1250 and 500 for short and long channel results, respectively. Also, the values $\mu = 1.0$ and thus $\alpha_U = 2.5 \cdot 10^4$ and $\alpha_L = 2.5 \cdot 10^{-4}$ are used. The final topologies are shown in Figure 4.

The optimization process for the short double channels problem took 1533.5 seconds to complete and 25 function evaluations were performed. The convergence curves for both cases can be seen in Figure 5. The corresponding values of the functional given by equation (2.10) are presented in Table 1.

In order to compare the results with the literature [12, 14] we define the functional

$$\mathcal{G}(u) = \int_\Omega \mu \|\nabla u\|^2 \,, \tag{7.1}$$

which does not have the porosity term. The comparison is shown in Table 2. The results are close to the analytical solution with small differences that can be addressed to the fact that the volume fraction (R_{vol}) is not exactly 0.33 as in the compared cases, given that it is hard to calibrate the β coefficient to get an exact volume ratio, however they are very close.

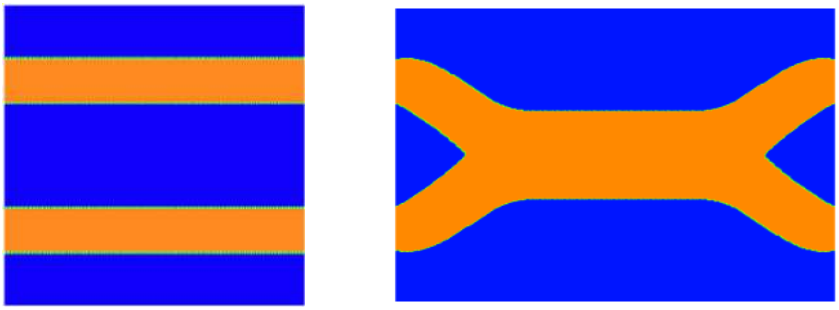

(a) (b)

FIGURE 4. Example 1. Final topologies for double channel problem considering Stokes formulation, $\mu = 1.0$ and $u_0 = 1.0$: short double channel $l = 1.0$ (a) and long double channel $l = 1.5$ (b).

TABLE 1. Example 1. Functional values for resulting topologies of Stokes short and long double channel problems ($\mu = 1.0$ and $u_0 = 1.0$)

		Short ($l = 1$)	Long ($l = 1.5$)
Stokes	$\mathcal{F}_\omega(u)$	205.29	147.78
	$\mathcal{J}(u)$	60.71	40.75
	$\lvert\omega\rvert$	0.29	0.54

TABLE 2. Example 1. Functional value comparison for resulting topologies of double channel problem ($\mu = 1.0$ and $u_0 = 1.0$).

	Short ($l = 1.0$)	Long ($l = 1.5$)
Case	$\mathcal{G}(u)$ / R_{vol}	$\mathcal{G}(u)$ / R_{vol}
Analytical	32.00 / 0.33	-
Figure 4	34.35 / 0.29	31.01 / 0.35
Borrvall & Petersson	25.67 / 0.33	27.64 / 0.33
Challis & Guest	31.68 / 0.33	32.86 / 0.33

7.2. **Example 2: Navier-Stokes Double Channel Problem.** The second implementation example aims to illustrate the behavior of the algorithm for the Navier-Stokes formulation considering low and high values of Reynolds number. The design domain is the same of Example 1 with $l = 1.5$ (Fig. 3). The objective is the minimization of energy dissipation between inlets and outlets. The domain is discretized with a regular mesh of 45,000 triangular elements. The values of 0.01 for μ and consequently 250.0 for α_U and $2.5 \cdot 10^{-6}$ for α_L are used.

As a result, a comparison of topologies generated by considering Navier-Stokes equations for low ($Re = 2$; $u_0 = 0.1$) and high ($Re = 200$; $u_0 = 10.0$) values of Reynolds number is presented. The value of the β coefficient is equal to 0.1 and 100.0 for low and high Reynolds number results, respectively. Figure 6 shows the final topologies. This topology optimization for high Reynolds number took 584.36 seconds to complete and 8 function evaluations were performed.

For the low Reynolds number ($Re = 2$), the topologies obtained by considering Stokes or Navier-Stokes equations are the same. It differs however from Example 1 because of the volume constraint (β parameter). The corresponding values of functionals given by equation (2.10) are presented in Table 3.

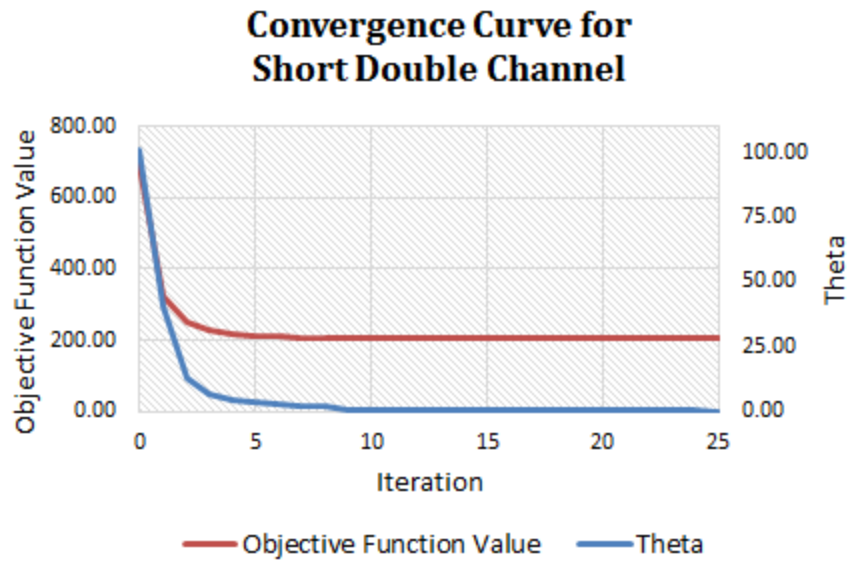

(a)

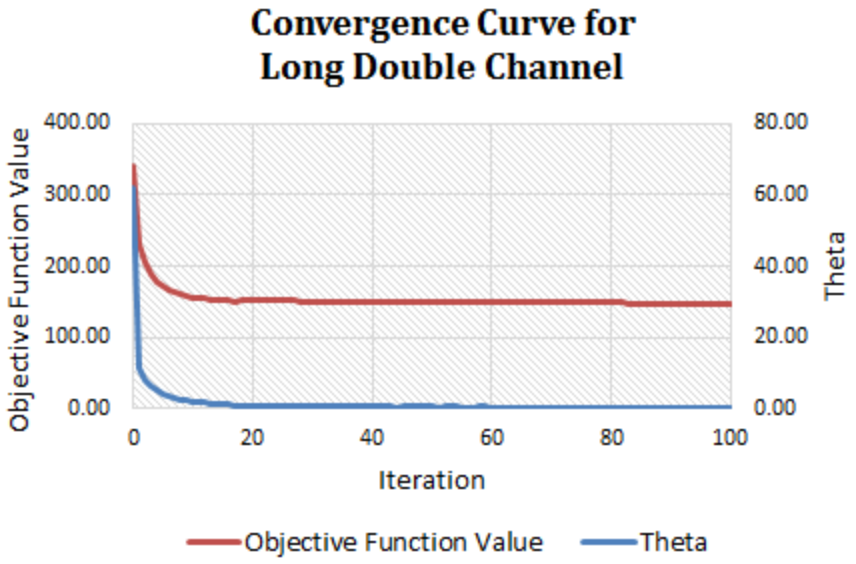

(b)

FIGURE 5. Example 1. Convergence curves for double channel problem considering Stokes formulation, $\mu = 1.0$ and $u_0 = 1.0$: short double channel $l = 1.0$ (a) and long double channel $l = 1.5$ (b).

TABLE 3. Example 2. Functional values for resulting topologies of double channel problem for low and high Reynold numbers ($\mu = 0.01$).

		$Re = 2$	$Re = 200$
Navier-Stokes	$\mathcal{F}_\omega(u)$	0.052	112.46
	$\mathcal{J}(u)$	0.014	43.01
	$\lvert\omega\rvert$	0.380	0.64

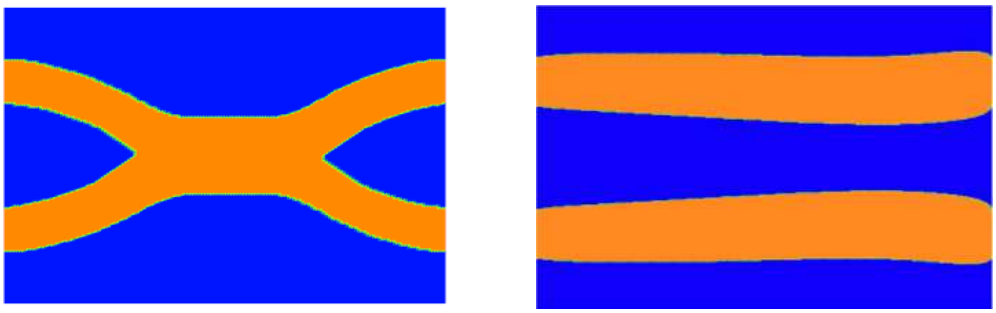

(a) (b)

FIGURE 6. Example 2. Final topologies for double channel problem (Navier-Stokes): low (a) and high Reynolds number (b).

7.3. **Example 3: Navier-Stokes Obstacle Problem.** The third implementation example is the channel design optimization problem by considering an obstacle. The corresponding design domain with an obstacle inside is shown in Figure 7. The objective is to minimize energy dissipation between the inlet and the outlet. In the follow results, the domain is discretized with a regular mesh of 59,000 triangular elements during the optimization procedure. In this case we use 0.01 for μ and consequently 250.0 for α_U and $2.5 \cdot 10^{-6}$ for α_L.

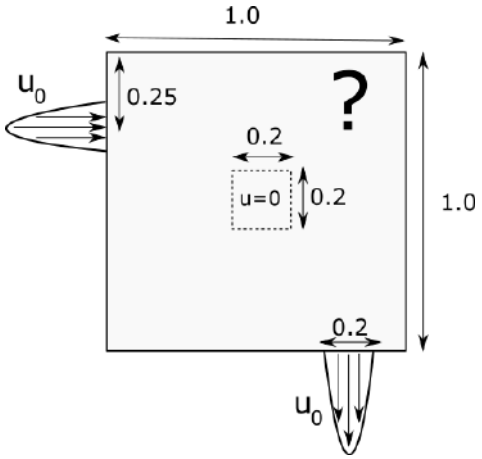

FIGURE 7. Example 3. Design domain for obstacle problem.

As a result, a comparison of topologies generated by considering Navier-Stokes equations with different initial domains is presented for low ($Re = 2$; $u_0 = 0.1$) values of Reynolds. The two initial domains are: one completely filled with fluid and another one composed by solid only. The value of β coefficient is equal to 0.06 for both cases. Figure 8 shows the sequence of topologies during the optimization until the convergence is reached for the fluid initialization. Figure 9 shows the final topologies obtained.

The topologies obtained by considering the fluid and solid initialization are quite different. They can be interpreted as two different local minima. The corresponding values of the functional given by equation (2.10) are presented in Table 4.

7.4. **Example 4: 3D Three-Way Channel Problem.** Now, by applying the methodology presented, the problem of a three-way channel is solved. This example considers a 3D domain with two fluid inlets of velocity with parabolic profiles, one normal to the x axis and the other one normal to the y axis, and one outlet, normal to the z axis. The corresponding design domain is shown in Figure 10. A boundary condition of pressure is imposed on the outlet with value of $p_0 = 0.0$, and the values of 0.01 for μ, 250.0 for α_U and $2.5 \cdot 10^{-6}$ for α_L are used. The objective is to minimize energy dissipation between the inlets and outlet. In the following results, the

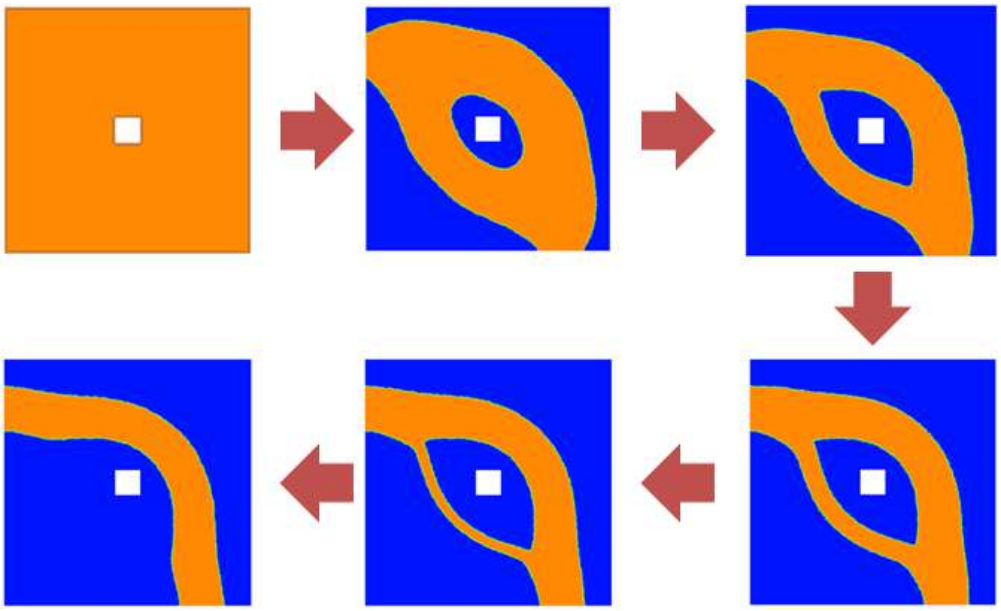

FIGURE 8. Example 3. Sequence of topologies during the optimization process for the obstacle problem considering fluid initialization.

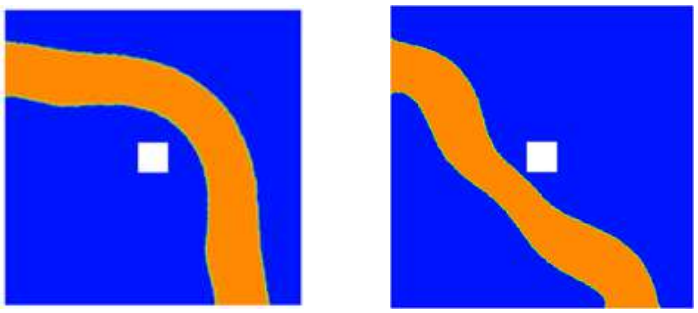

(a) (b)

FIGURE 9. Example 3. Final topologies for obstacle problem: fluid initialization (a) and solid initialization (b).

TABLE 4. Example 3. Functional values for resulting topologies of obstacle problem for different initializations ($\mu = 0.01$ and $u_0 = 0.1$).

		Fluid Initialization	Solid Initialization
Navier-Stokes	$\mathcal{F}_\omega(u)$	0.019	0.017
	$\mathcal{J}(u)$	0.0072	0.0054
	$\lvert\omega\rvert$	0.20	0.19

domain is discretized with a regular mesh of 96,000 tetrahedral elements during the optimization procedure.

The results derived from considering Stokes equations and an intermediate value of Reynolds number ($Re = 40$; $u_0 = 1.0$) to facilitate the convergence. The value of the β coefficient is equal to 1.0. Figure 11 shows the final topologies obtained with this configuration, in which the values of the shape functionals are given by $\mathcal{F}_\omega(u) = 1.6768$ and $\mathcal{J}(u) = 0.6463$. The convergence curve is similar to that of the previous problem.

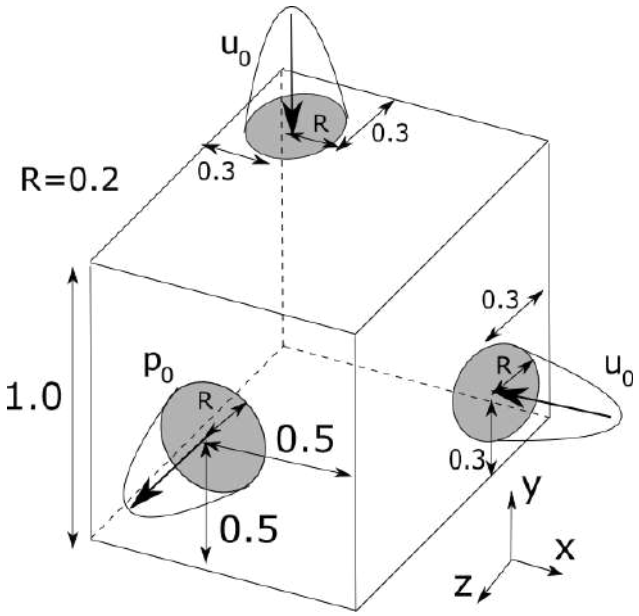

FIGURE 10. Example 4. Design domain for 3D three way channel problem.

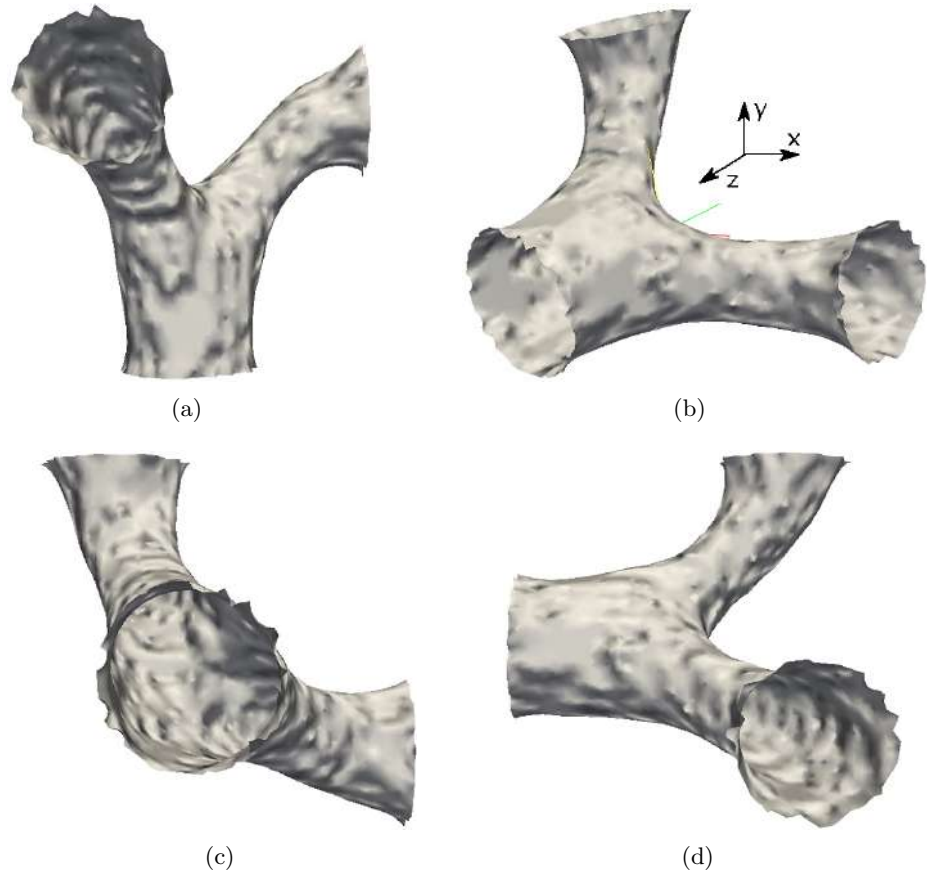

(a) (b)

(c) (d)

FIGURE 11. Example 4. Final topologies (fluid domain) for the 3D cross channel problem obtained by considering the Stokes system with inlet parabolic velocity: Y view (a), isometric view (b), Z view (c) and X view (d).

7.5. **Example 5: 3D Cross Channel Problem.** Finally, considering the stokes formulation, the problem of a 3D cross channel is solved. This example considers a 3D domain with two fluid

inlets and two outlets, both normal to the z axis. The corresponding design domain is shown in Figure 12, in which the velocities have parabolic profiles. The objective is to minimize the energy dissipation between the inlets and outlet. In the results as follows, the domain is discretized with a regular mesh of 99,000 tetrahedral elements during the optimization procedure.

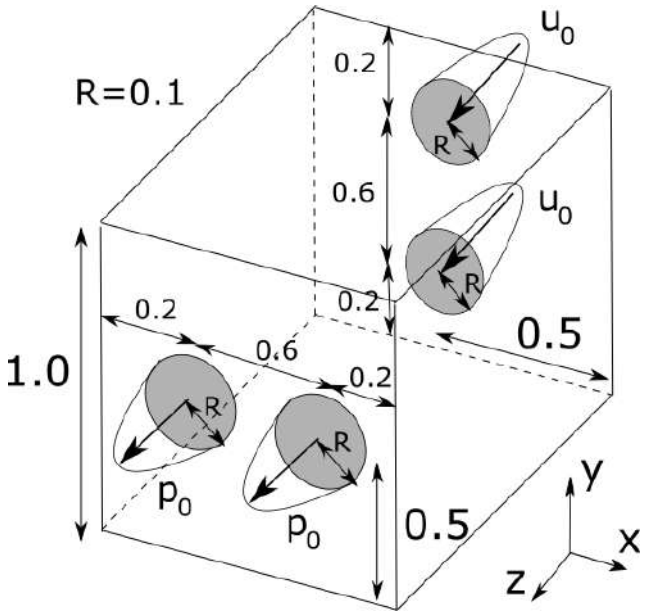

FIGURE 12. Example 5. Design domain for 3D cross channel problem.

The results are obtained by considering Stokes equations, and values of 0.01 for μ, 250.0 for α_U, $2.5 \cdot 10^{-6}$ for α_L and an intermediate value of Reynolds number ($Re = 20$; $u_0 = 1.0$). Also, a boundary condition of pressure is imposed on the outlet with value of $p_0 = 0.0$. The value of the β coefficient is equal to 1.0. Figure 13 shows the final topologies obtained with this configuration, in which the respective values of the shape functionals are $\mathcal{F}_\omega(u) = 0.3108$ and $\mathcal{J}(u) = 0.2182$.

8. Conclusions

We developed a topological derivative formulation for fluid channel design based on the concept of traditional topology optimization formulations in which solid or fluid material is distributed at each point of the domain to optimize the cost function and to satisfy constraints. Since inclusions mimicking solid or fluid phase are created instead of inserting or removing holes, this strategy solved the numerical difficulty of previous topological derivative formulations in which the boundary conditions on the holes have to be handled during the optimization process. Moreover, in contrast to traditional topology optimization methods, the topological derivative formulation does not require a material model concept based on intermediary porosities. Thus, interpolation schemes are unnecessary. In addition, the topological derivative has the advantage of providing an analytical form for the topological sensitivity which allows obtaining the optimal design in a few iterations. Therefore, the resulting topology optimization algorithm is remarkably efficient and of simple computational implementation. In fact, it converges very quickly and features only a minimal number of user-defined algorithmic parameters.

In particular, the theoretical results are used to devise a topology optimization algorithm based on the topological derivative together with a level-set domain representation method, as proposed in [7]. The remarkable simplicity of the closed forms sensitivities (3.25) for Stokes and (4.19) for Navier-Stokes systems is to be noted. Since in this particular case the topological derivatives are independent of the polarization tensor, they could be derived using standard arguments. In any case, our derivations are general and could be applied to more complicated situations, such as the problems in which the polarization tensor plays a key role [10].

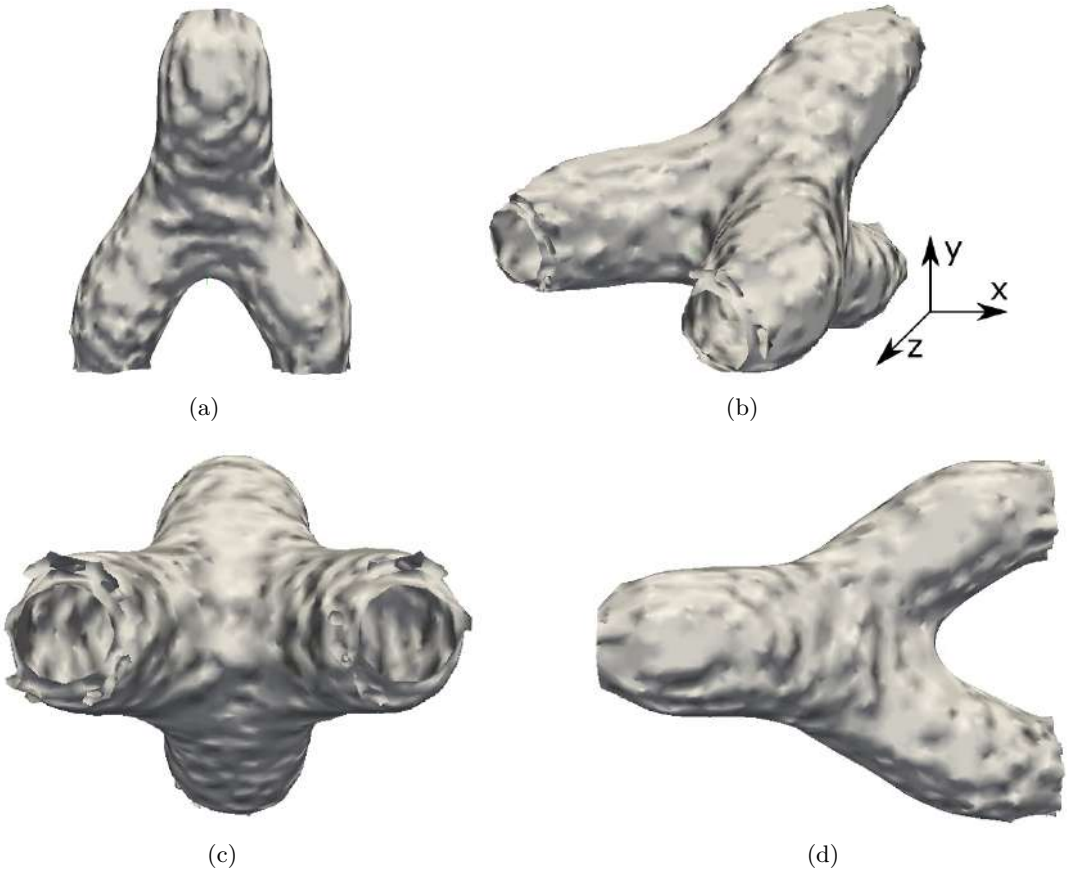

FIGURE 13. Final topologies (fluid domain) for the 3D cross channel problem obtained by considering the Stokes system with inlet parabolic velocity: Y view (a), isometric view (b), Z view (c) and X view (d).

To evaluate the formulation, the minimization of the energy dissipation in two-dimensional double and with obstacle channels as well as three-dimensional cross and three-way channel designs have been presented, which confirm the generality of the method. Results from considering Stokes and Navier-Stokes equations in two and Stokes in three spatial dimensions are presented and compared. The topologies with well defined solid/fluid interfaces are obtained in a few iterations (even for 3D problems). This shows that the proposed formulation based on the topological derivative concept is robust and consistent with existing topology optimization methods based on material models.

However, current, the algorithm solves the governing equations (Stokes or Navier-Stokes) every function evaluation which is not so efficient if a nonlinear governing equation (such as Navier-Stokes) is considered. This limits the application of this algorithm for large computational problems. Thus, as a future work, it can be implemented a onestep approach where the governing equations and line search would be solved simultaneously [32, 18].

ACKNOWLEDGEMENTS

This research was partly supported by CNPq (Brazilian Research Council), FAPERJ (Research Foundation of the State of Rio de Janeiro) and FAPESP (Sao Paulo Research Foundation). The authors thank the supporting institutions. The first author thanks the financial support of FAPESP under grants 2015/15189-7 and 2013/24434-0. The fourth author thanks the financial support of CNPq (National Council for Research and Development) under grant 304121/2013-4.

References

[1] G. Allaire, F. Jouve, and N. Van Goethem. Damage and fracture evolution in brittle materials by shape optimization methods. *Journal of Computational Physics*, 230(12):5010–5044, 2011.

[2] Martin S. Alnæs, Anders Logg, Kristian B. Ølgaard, Marie E. Rognes, and Garth N. Wells. Unified form language. *ACM Transactions on Mathematical Software*, 40(2):1–37, mar 2014.

[3] M.S. Alnaes, Anders Logg, K A. Mardal, Ola Skavhaug, and H.P. Langtangen. Unified framework for finite element assembly. *International Journal of Computational Science and Engineering*, 4(4):231–244, may 2009.

[4] Patrick R. Amestoy, Iain S. Duff, Jean-Yves L'Excellent, and Jacko Koster. A Fully Asynchronous Multifrontal Solver Using Distributed Dynamic Scheduling. *SIAM Journal on Matrix Analysis and Applications*, 23(1):15–41, jan 2001.

[5] S. Amstutz. The topological asymptotic for the Navier-Stokes equations. *ESAIM: Control, Optimisation and Calculus of Variations*, 11(3):401–425, 2005.

[6] S. Amstutz. Analysis of a level set method for topology optimization. *Optimization Methods and Software*, 26(4-5):555–573, 2011.

[7] S. Amstutz and H. Andrä. A new algorithm for topology optimization using a level-set method. *Journal of Computational Physics*, 216(2):573–588, 2006.

[8] S. Amstutz, S. M. Giusti, A. A. Novotny, and E. A. de Souza Neto. Topological derivative for multi-scale linear elasticity models applied to the synthesis of microstructures. *International Journal for Numerical Methods in Engineering*, 84:733–756, 2010.

[9] S. Amstutz, A. A. Novotny, and E. A. de Souza Neto. Topological derivative-based topology optimization of structures subject to Drucker-Prager stress constraints. *Computer Methods in Applied Mechanics and Engineering*, 233–236:123–136, 2012.

[10] S. Amstutz, A. A. Novotny, and N. Van Goethem. Topological sensitivity analysis for elliptic differential operators of order $2m$. *Journal of Differential Equations*, 256:1735–1770, 2014.

[11] M. Bergounioux and Y. Privat. Shape optimization with stokes constraints over the set of axisymmetric domains. *SIAM J. Control Optim.*, 51(1):599–628, 2013.

[12] T. Borrvall and J. Petersson. Topology optimization of fluids in stokes flow. *International Journal for Numerical Methods in Engineering*, 41(1):77–107, 2003.

[13] D. E. Campeão, S. M. Giusti, and A. A. Novotny. Topology design of plates consedering different volume control methods. *Engineering Computations*, 31(5):826–842, 2014.

[14] V. J. Challis and J. K. Guest. Level set topology optimization of fluids in stokes flow. *International Journal for Numerical Methods in Engineering*, 79:1284–1308, 2009.

[15] R. Dautray and J. L. Lions. *Mathematical analysis and numerical methods for science and technology. Volume 2 – Functional and Variational Methods*. Springer, Berlin, Heidelberg, New York, 1988.

[16] X. Duan and F. Li. Material distribution resembled level set method for optimal shape design of stokes flow. *Applied Mathematics and Computation*, 266:21–30, 2015.

[17] A. Evgrafov. The limits porous materials in the topology optimization of stokes flows. *Applied Mathematics and Optimization*, 52(3):263–277, 2005.

[18] A. Evgrafov. On chebyshevs method for topology optimization of stokes flows. *Structural and Multidisciplinary Optimization*, 51(4):801–811, 2015.

[19] A. Gersborg-Hansen. Topology optimization of incompressible newtonian flows at moderate reynolds numbers. Master's thesis, Technical University of Denmark. Department of Mechanical Engineering Solid mechanics, Lyngby, 2003.

[20] A. Gersborg-Hansen. *Topology optimization of incompressible newtonian flows at moderate Reynolds numbers*. PhD thesis, Technical University of Denmark. Department of Mechanical Engineering Solid mechanics, Lyngby, 2007.

[21] A. Gersborg-Hansen, O. Sigmund, and R. B. Haber. Topology optimization of chanel flow problems. *Struct. Multidisc. Optim.*, 90:90–120, 2005.

[22] J. Guest and J. Prevost. Topology optimization of creeping fluid flows using a darcy and stokes flow. *International Journal for Numerical Methods in Engineering*, 69:1374–1404, 2007.

[23] PH. Guillaume and M. Hassine. Removing holes in topological shape optimization. *ESAIM: Control, Optimisation and Calculus of Variations*, 14(1):160–191, 2008.

[24] Ph. Guillaume and K. S. Idris. Topological sensitivity and shape optimization for the stokes equations. *SIAM J. Control Optim.*, 43(1):1–31, 2004.

[25] E. J. Haug, K. K. Choi, and V. Komkov. *Desing sensitivity analysis of structural systems*. Academic Press, New York, 1986.

[26] M. Hintermüller and A. Laurain. Multiphase image segmentation and modulation recovery based on shape and topological sensitivity. *Journal of Mathematical Imaging and Vision*, 35:1–22, 2009.

[27] M. Hintermüller, A. Laurain, and A. A. Novotny. Second-order topological expansion for electrical impedance tomography. *Advances in Computational Mathematics*, 36(2):235–265, 2012.

[28] H. Lebesgue. Sur l'intégration des fonctions discontinues. *Annales Scientifiques de l'École Normale Supérieure*, 27:361–450, 1910.

[29] Anders Logg and Garth N. Wells. DOLFIN: Automated Finite Element Computing. *ACM Transactions on Mathematical Software*, 37(2):1–28, apr 2010.

[30] Anders Logg, Garth N Wells, and The Fenics Book. *Automated Solution of Differential Equations by the Finite Element Method*, volume 84 of *Lecture Notes in Computational Science and Engineering*. Springer Berlin Heidelberg, Berlin, Heidelberg, 2012.

[31] A. A. Novotny and J. Sokołowski. *Topological derivatives in shape optimization*. Interaction of Mechanics and Mathematics. Springer, 2013.

[32] C. Othmer. A continuous adjoint formulation for the computation of topological and surface sensitivities of ducted flows. *International Journal for Numerical Methods in Fluids*, 58:861–877, 2008.

[33] E.M. Papoutsis-Kiachagias, E.A. Kontoleontos, A.S. Zymaris, D.I. Papadimitriou, and K.C. Giannakoglou. Constrained topology optimization for laminar and turbulent flows, including heat transfer. *Evolutionary and Deterministic Methods for Design, Optimization and Control, Symposium Proceedings*, 2011.

[34] P. Plotnikov and J. Sokołowski. *Compressible Navier-Stokes Equations. Theory and shape optimization*. Springer-Verlag, Basel, 2012.

[35] J. Sokołowski and A. Żochowski. On the topological derivative in shape optimization. *SIAM Journal on Control and Optimization*, 37(4):1251–1272, 1999.

[36] R. Temam. *Navier-Stokes Equations: Theory and Numerical Analysis*. North-Holland, Amsterdam, 1984.

[37] N. Van Goethem and A. A. Novotny. Crack nucleation sensitivity analysis. *Mathematical Methods in the Applied Sciences*, 33(16):197–1994, 2010.

[38] N. Wiker, A. Klarbring, and T. Borvall. Topology optimization of regions of darcy-stokes finite element. *International Journal for Numerical Methods in Engineering*, 66:461–484, 2006.

(A.A. Novotny) Laboratório Nacional de Computação Científica LNCC/MCT, Coordenação de Matemática Aplicada e Computacional, Av. Getúlio Vargas 333, 25651-075 Petrópolis - RJ, Brasil

E-mail address: novotny@lncc.br

(L.F.N. Sá, R.C.R. Amigo and E.C.N. Silva) Department of Mechatronics and Mechanical Systems Engineering of Escola Politecnica, University of Sao Paulo, Av. Prof. Mello Moraes, 2231 - 05508-030, Sao Paulo, Brazil

E-mail address: luis.sa@usp.br, ricardo.amigo@usp.br, ecnsilva@usp.br